Renewable Energy 242 (2025) 122389

Contents lists available at ScienceDirect

Renewable Energy

journal homepage: www.elsevier.com/locate/renene

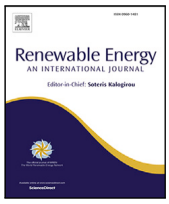

Effects of tip gap size and aspect ratio on the performance of a Wells turbine

Fabio Licheri *, Tiziano Ghisu, Francesco Cambuli, Pierpaolo Puddu, Mario Carta

Department of Mechanical, Chemical and Materials Engineering, University of Cagliari, via Marengo 2, 09123 Cagliari, Italy

ARTICLE INFO

Keywords:
OWC systems
Wells turbines
Experimental analysis
Tip clearance effect
Aspect-ratio effect
Reynolds' number effect

ABSTRACT

The Wells turbine is one of the most suitable power take offs for oscillating water column systems, due to its simple and effective design combined to a reasonable efficiency. In recent years, a significant number of local geometry modifications have been suggested, with the promise to provide some important performance improvements. In order to achieve the full potential of this machine, these local modifications need to be applied to an optimal configuration of the machine's global geometric parameters, such as tip clearance, blade aspect ratio, hub-to-tip ratio and solidity.

The aim of this work is to provide a comprehensive experimental analysis of the effects of aspect ratio and tip clearance on the overall performance and operating range of a Wells turbine. These two effects have been accurately isolated, excluding the influence of the Reynolds' number, thus providing a larger and more detailed set of data with respect to the ones available in the literature. An important conclusion is that the tip clearance size, which plays a dominant role, is best expressed in non-dimensional form with respect to the blade height rather than to the blade chord. With this approach, the turbine performance appears independent from the blade aspect ratio, within the ranges of parameters analyzed in this work. A lower aspect ratio, however, helps to achieve a larger operational Reynolds' number, leading to better overall performance.

1. Introduction

Ongoing energy transition programs [1] are drawing the attention of researchers to sea wave energy, due to its large availability even in less energetic seas, such as the Mediterranean [2,3]. Different wave energy converter (WEC) technologies have been proposed and studied in recent years [4], and solutions based on the Oscillating Water Column (OWC) principle are considered as the most interesting. Their strength lies in the absence of moving parts interacting with the sea water, resulting in highly reliable devices, simple to construct and easy to maintain [5]. An OWC device, schematically represented in Fig. 1(a), is composed of two parts: a chamber, open at the bottom, where the wave potential energy is converted into the pneumatic energy of a bi-directional airflow; a power take off (PTO) system, which commonly consists of an air turbine moved by this airflow, is employed to produce mechanical energy at its shaft. The PTO is connected to an electric generator to finally convert mechanical energy into electricity.

The Wells air turbine [6], represented in Fig. 1(b), is one of the most suitable turbomachine to have been coupled with an OWC system [7], due to its simplicity of construction and high reliability, in combination with a reasonable turbine efficiency. These characteristics are achieved thanks to the self-rectifying behavior that allows the same direction of rotation to be maintained regardless of the flow direction. This property is obtained using a symmetric blade profile, staggered at 90 degrees with respect to the axis of rotation, as sketched in Fig. 1(b).

The simple geometry comes with some limitations (a poor torque at low incidence angles and a limited operating range due to stall) and introduces strong constraints to the aerodynamic design of the blade (the symmetry with respect to the chord that is necessary to obtain the self-rectifying behavior). In light of the above, improved rotor solutions have been typically researched through the modification of the global geometric parameters of the rotor, i.e. the tip gap size and configuration [8–14], the hub-to-tip ratio [11,15], the rotor solidity [8,16–18], the blade aspect ratio [19] and the blade profile thickness [12,17]. In addition, several local modifications have also been proposed, such as end plates [20], trailing edge refined shapes [21], suction slots [22], profile optimization [23], variable thickness along the blade span [24], radiused tip [25], gurney flaps [26] and stall fences [27].

A limited number of works have provided useful correlations between the turbine's parameters and its performance and operating range. Most of these correlations have been summarized by Raghunathan in [19], where the mean cycle efficiency and the maximum flow coefficient (in the absence of stall) have been related to the above geometric parameters on the basis of experimental data. These correlations have been used abundantly after their introduction in early

* Corresponding author.
E-mail addresses: fabio.licheri@unica.it (F. Licheri), tiziano.ghisu@unica.it (T. Ghisu), francesco.cambuli@unica.it (F. Cambuli), pierpaolo.puddu@unica.it (P. Puddu), mario.carta@unica.it (M. Carta).

https://doi.org/10.1016/j.renene.2025.122389
Received 12 June 2024; Received in revised form 29 November 2024; Accepted 9 January 2025
Available online 18 January 2025

Nomenclature

Acronyms

BDC	Bottom dead center
OWC	Oscillating water column
PTO	Power take off
TDC	Top dead center
UPM	Uncertainty propagation method

Dimensional properties

A	Area
α	Angle of the absolute flow
β	Angle of the relative flow
C	Absolute velocity
c	Blade chord
C^*	Reference velocity
D	Turbine diameter
f	Frequency
h	Blade height
μ	Dynamic viscosity
Ω	Angular rotational frequency
p	Pressure
Q	Volumetric flow rate
r	Turbine radius
ρ	Air density
t	Tip clearance
$\mathcal{T}$	Torque
T_w	Piston period
U	Peripheral rotor speed
V	Velocity
W	Relative velocity
Z	Piston position

Non-dimensional properties

AR	Aspect ratio
η	Efficiency
ν	Hub-to-tip ratio
p^*	Pressure drop coefficient
ϕ	Flow coefficient
Re	Reynolds' number
σ	Rotor solidity
$\mathcal{T}^*$	Torque coefficient
t_c	Tip gap-to-chord ratio
t_h	Tip gap-to-height ratio
ξ_R	Loss coefficient related to the viscous losses
ξ_{EX}	Loss coefficient related to the exit kinetic energy
z	Number of blades
$Z^* = {(Z-Z_{BDC})}/{(Z_{TDC}-Z_{BDC})}$	Non-dimensional piston position

Subscripts and superscripts

1	Inlet
2	Outlet
$casing$	Turbine casing
f	Flow
hub	Turbine hub
$\overline{()}$	Mean/averaged value
s	Stall
tip	Turbine tip
ts	Total to static
z	Axial direction

'90s, also for the validation of numerical simulations. The definition of correlations for rotor performance caused by geometry modifications is crucial both for designing and coupling a Wells rotor with an OWC system, often with a specific installation site in mind. Wave-to-wire models are useful for the evaluation of energy conversion stages from the available wave power to the output electric power at the generator. Most of these models often adopt empirical models for turbine performance [28–31]. The availability of a larger basis of experimental data to complement and extend the available ones [19], now quite outdated, both based on laboratory measurements such as the ones presented in this work and on-site evaluations [32], is crucial for the development of reliable models to be used in global system evaluations. In addition, these detailed experimental data could serve for the validation of numerical simulations, that could the be used to extend the available data.

The effect of the tip gap size has been evaluated numerically in [9,10], showing a good agreement with the experiments in [19] only in terms of general trends, but not in terms of actual values. The tip gap size has been observed to play an important role on the stall point [14], due to the presence of a leakage flow that energizes the suction side flow near the blade, thus delaying separation. This is obtained at the price of a reduction in the rotor efficiency for the same operating condition [19]. A correct selection of the tip gap size is then fundamental when matching a Wells turbine with the wave energy characteristic, in order to obtain the maximum performance. All the analyses on the tip clearance size have treated this parameter in non-dimensional form, dividing the tip gap by the blade chord (t_c) [13,14,19]. The effect of the blade aspect ratio (AR), has also been analyzed [19], but with some limitations on the methodology adopted, as pointed out by the authors, due to the challenges linked to isolating its effect from the ones due to the other geometric and flow parameters.

In light of the above limitations, this paper aims to provide a useful set of data to assist the design of a Wells turbine and of the overall OWC system, extending the investigation of the effects of tip clearance size and blade aspect ratio on the performance of a laboratory-scale rotor. The separation between these two effects (and other effects, such as the Reynolds' number) has been strictly preserved in the present investigation, by means of a carefully planned design of experiment, making use of a total number of 9 different rotors. All the analyses have been conducted under regular wave conditions reproduced within an OWC simulator. Global measurements have been performed on these rotor geometries and used to define their performance in a wide operating range including stall. The results of the present investigations will also provide a set of characteristic curves for different rotor geometries that can be directly introduced in existing wave-to-wire models for the evaluation of an OWC systems that uses a Wells turbine as PTO. This paper is organized as follows: the performance definition and the experimental design are described in Section 2, while all the information on the instrumentation and methodologies are reported in detail in Section 3; results are presented and discussed in Section 4; finally, conclusions are drawn in Section 5.

2. Methodology

2.1. Performance definition

The performance of any turbomachine can be expressed in non-dimensional form [33,34], as suggested by similarity laws, in order

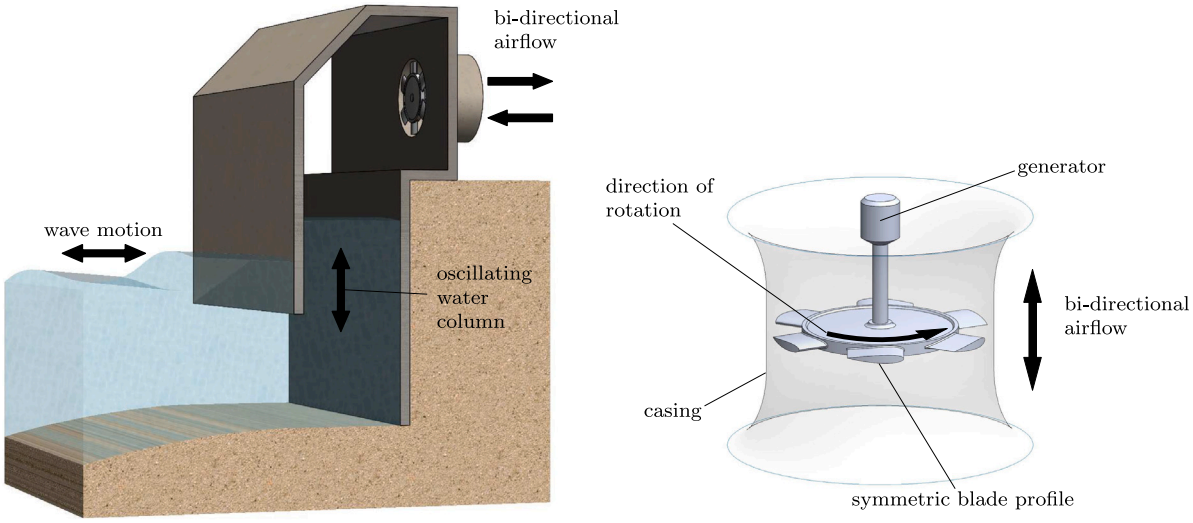

(a) OWC working principle (b) Wells turbine operating principle.

Fig. 1. Working principle of an on-shore OWC device with Wells turbine.

to reduce the number of independent parameters required to describe them. For a Wells turbine, the following non-dimensional parameters are typically defined and adopted [35,36] for its complete characterization: the flow coefficient ϕ, the torque coefficient $\mathcal{T}^*$ and the pressure coefficient p^*.

$$\phi = \frac{C_z}{\Omega r_{tip}} \qquad \mathcal{T}^* = \frac{\mathcal{T}}{\rho \Omega^2 r_{tip}^5} \qquad p^* = \frac{\Delta p}{\rho \Omega^2 r_{tip}^2} \tag{1}$$

where C_z is the axial flow velocity at the turbine inlet and Δp is the static pressure difference across the turbine. Based on these parameters, the turbine efficiency can be calculated as follows:

$$\eta = \frac{\mathcal{T}\Omega}{\Delta p Q} = \frac{\mathcal{T}^*}{p^* \phi} \frac{1}{\pi(1-\nu^2)} \tag{2}$$

where ν is the hub-to-tip ratio of the rotor.

The above non-dimensional parameters can be evaluated using only global measurements, i.e. the turbine's rotational speed (Ω) and its output torque ($\mathcal{T}$), the wall static pressures drop (Δp) across the turbine and the flow rate (Q). This approach does not require local flow measurements, and is widely adopted in experimental investigations [35,37,38], even though the total pressure often replaces the static pressure drop.

It should be noted that the Wells turbine performance expressed in non-dimensional form (p^*, $\mathcal{T}^*$ and η) is a function not only of the geometry and of the operating point, but also of the flow conditions typically expressed in non-dimensional form through Mach and Reynolds' (Re) numbers. In this work, compressibility effects have not been considered, as the turbine operates at a maximum Mach number of about 0.15. The effects of the Reynolds' number have been isolated from the effect of the geometry by carefully designing the experiments in order to have the same value of the Reynolds' number (1.3×10^5). Finally, the effects of this important parameter have then been considered separately on three turbine geometries (Section 4).

In this experimental work, the flow rate through the turbine has been calculated based on the piston velocity, accounting for the temporal delay due to the presence of the OWC chamber [39]. The output torque has been cleared from windage and friction losses and from the rotor inertial torque, based on a characterization of the rotor under no flow conditions. This approach allows to take into consideration only the aerodynamic behavior of the Wells rotor, removing the effects associated to its inertia and the bearing friction. The non-dimensional torque coefficient is therefore calculated using the aerodynamic torque, and the resulting rotor efficiency (Eq. (2)) represents the aerodynamic efficiency of the turbine, as shown in [40]. Nonetheless, a more appropriate efficiency measure can be defined employing the total-to-static pressure drop across the turbine, in order to consider the actual energy balance through the machine. This formulation, expressed in Eq. (3), requires the evaluation of the inlet total pressure p_{01}, which is not directly available from the above global measurements.

$$\eta_{ts} = \frac{\mathcal{T}\Omega}{(p_{01} - p_2)Q} = 1 - \xi_R - \xi_{EX} \tag{3}$$

For a fully axial flow coming from the ambient side into the OWC chamber, generally referred as the inflow phase, p_{01} can be approximated with the ambient static pressure, assuming inlet duct pressure losses negligible [41]. Typical velocity triangles at the inlet and outlet of turbine during this phase are sketched in Fig. 2.

In a previous work [41], the authors decomposed the losses inside a Wells turbine by introducing two coefficients related to viscous losses, ξ_R, and to the exit kinetic energy, ξ_{EX}, as often done in other more common turbomachinery [42]. A methodology to calculate these two parameters using only global measurements has been proposed in [41] and it is strictly valid only for the inflow phase, when the flow is fully axial [43,44]. With this assumption, the loss coefficients can be calculated as follows [41]:

$$\xi_R = (1 - \psi^2)(1 + \lambda^2) \tag{4}$$

$$\xi_{EX} = \lambda^2 + \psi^2(1 + \lambda^2) - 2\psi\lambda\cos(\beta_2)\sqrt{1 + \lambda^2} \tag{5}$$

Eqs. (4) and (5) show that the loss coefficients depend on the operating conditions, i.e. the velocity coefficient $\lambda = U/C^*$, and on the aerodynamic losses, represented by the relative velocity reduction coefficient $\psi = W_2/W_{2s}$. The velocity coefficient is defined introducing the reference velocity C^*, that can be related to the total-to-static pressure drop ($C^{*2}/2 = (p_{01} - p_2)/\rho$) and then is used to evaluate the isentropic relative velocity $W_{2,s}^2 = W_1^2 + C^{*2} - C_1^2$. In addition, the discharge loss coefficient is also affected by the relative outlet flow angle β_2. For a complete description of loss coefficients definitions, the interested reader is referred to [41].

2.2. Design of the Experiment (DoE)

The most relevant geometric parameters for designing Wells turbine rotors have been identified by Raghunathan [19]. They are: the solidity

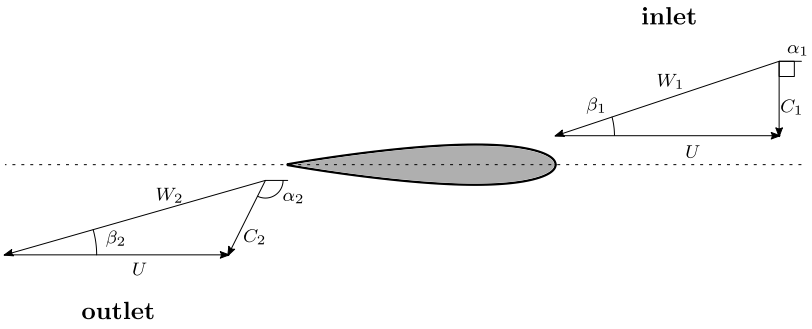

Fig. 2. Velocity triangles for a Wells turbine with fully axial inlet flow.

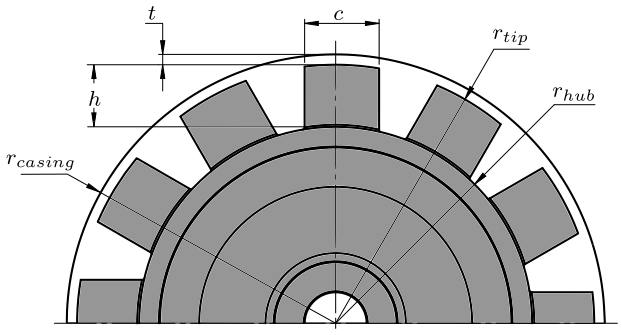

Fig. 3. Schematic view of a Wells rotor.

Table 1
Design of the experiment. Geometric parameters of the tested rotors.

Test	Rotor	t_c [%]	c [mm]	z	AR	$\overline{AR}$	σ	ν
1		0.5	72.0	6	0.426		0.623	0.756
2	1	1.5	72.0	6	0.416	0.42	0.625	0.761
3		2.5	72.0	6	0.406		0.627	0.765
4		0.5	43.2	10	0.713		0.623	0.755
5	2	1.5	43.2	10	0.703	0.70	0.624	0.758
6		2.5	43.2	10	0.693		0.625	0.761
7		0.5	30.9	14	0.998		0.623	0.755
8	3	1.5	30.9	14	0.988	0.99	0.624	0.757
9		2.5	30.9	14	0.978		0.625	0.759

σ, the hub-to-tip ratio ν, the aspect ratio AR, the tip clearance t, the aerofoil thickness ratio and the blade offset. Eq. (6) defines these parameters, with the exception of the last two which have been kept fixed in the present work (to 15% and 0 degrees, respectively) while Fig. 3 shows a schematic view of a Wells rotor to help their identification.

$$\sigma = \frac{A_{bld}}{A_{tot}} = \frac{hcz}{\pi r_{tip}^2(1-\nu^2)} \qquad \nu = \frac{r_{hub}}{r_{tip}} \qquad AR = \frac{h}{c} \qquad t_c = \frac{t}{c_{tip}} \tag{6}$$

where the solidity is generally defined as the ratio between the blade area (A_{bld}) and the rotor annulus area (A_{tot}) and the tip clearance is typically non-dimensionalized by means of the chord length at the tip radius c_{tip}, even though the chord does not vary along the blade height in traditional Wells turbine's blades. The hub-to-tip ratio (ν) is defined as the ratio between hub and tip radii (r_{hub} and r_{tip}) and the aspect ratio (AR) as the ratio between blade height (h) and chord (c).

In order to investigate the effects of t_c and AR variations on the performance, an experimental campaign has been conducted on a prototype Wells turbine while preserving the casing radius, r_{casing} = 126 mm, the hub radius, r_{hub} = 95 mm, the blade profile (NACA 0015) and its sweep ratio equal to 0.417 (15/36). In light of the above, the blade solidity and the hub-to-tip ratio have been maintained almost constant during the different experimental tests, as reported in Table 1. A full factorial DoE with a total number of 9 points has been chosen.

The ranges of variation of the selected parameters, i.e t_c and AR, have been chosen to be similar to the ones proposed in [19], where values of 0.5 was suggested for the AR (although values from 0.7 to 1 have been typically adopted [45–48]) and values lower than 2% were recommended for t_c [49]. Three values have been considered for both the tip clearance and the aspect ratio. This choice was considered a compromise between the exploration of the design space and the complexity of the experimental campaign. It should be noted that it is not easy or, sometimes, even possible to vary a single parameter while keeping the others constant. With this in mind, the maximum variation of AR for rotors with different tip gap sizes, t_c, is lower than 2.5%, hence the influence on turbine performance can be reasonably neglected. A mean value of the blade aspect ratio, $\overline{AR}$, has been therefore assigned for all cases with different tip gap sizes. Also the rotor solidity and the hub-to-tip ratio value variations are reasonably small and their influence on performance can be reasonably considered negligible with respect to the other parameters of interest.

3. Experimental setup and instrumentation

The OWC simulator housed at the DIMCM has been built in the early 1990s, and it has recently been upgraded with some significant modifications [41,50]. Its main parts are reproduced in Fig. 4, together with a close-up view of the measuring section where the turbine is housed.

The OWC simulator is composed of a cylindrical steel chamber where a piston, driven by a hydraulic unit, reproduces the periodic motion of a water column inside an OWC. Different wave states can be simulated in this experimental setup by changing the amplitude and frequency of the periodic motion of the piston, allowing a maximum flow speed of about 20 m/s at the inlet of the rotor. The piston displacement law set for the present analysis, a regular sinusoidal motion, is represented in Fig. 5, together with a typical flow coefficient obtained at the inlet section the rotor (the latter depends both on the piston displacement and the turbine speed, as defined in Eq. (1)).

A linear wire potentiometer is employed to measure the piston displacement and for feedback control of the hydraulic unit. Above the chamber, a Wells turbine, connected to an electric motor/generator controlled by an inverter with encoder feedback, is installed. Three rotors, with different ARs, have been built to perform the 9 tests of Table 1. Pictures are shown in Fig. 6. The metal hub is made of an aluminum alloy (Ergal 7075) and it is the same for each rotor configuration. The latter are obtained by fitting a different number of blades to the hub, as listed in Table 1. Each blade is made of a 3D printed resin and the external radius of the rotor is adjusted with a lathe processing, in order to accurately control the tip clearance value.

A shaft-to-shaft torque sensor is placed between the turbine and the electric motor, and it also allows to measure the turbine rotational speed with a built-in optical encoder. The measuring section

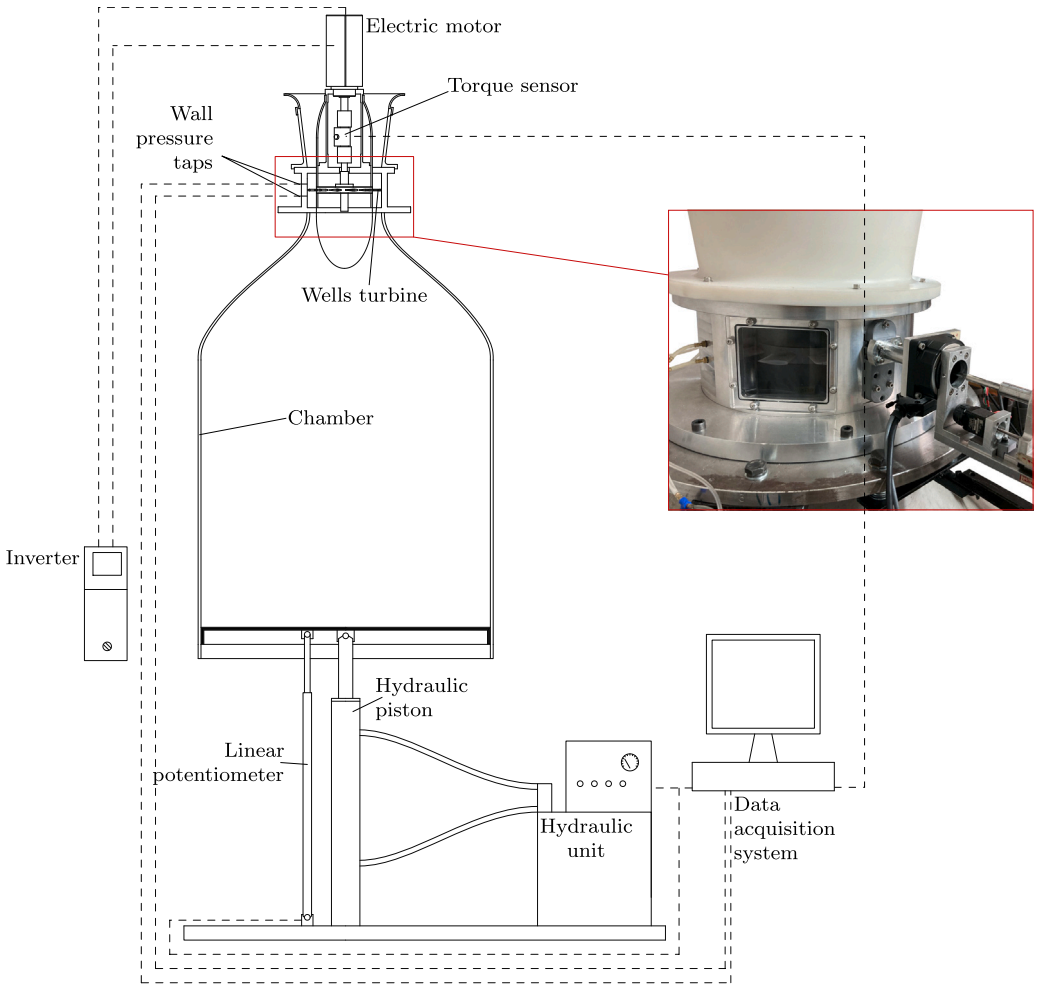

Fig. 4. Experimental setup scheme and measuring section.

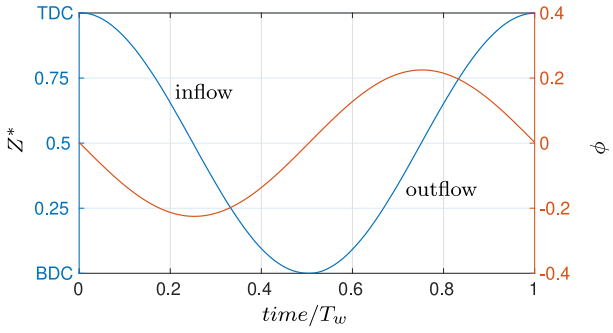

Fig. 5. Non-dimensional piston motion and flow speed for regular wave conditions.

is equipped with wall pressure taps placed on both rotor sides at a distance of ±7.5 mm from the blade chord. The volumetric flow rate cannot be directly measured with standardized measuring instruments, due to the configuration of the setup, but it can be derived from the piston motion (measured with the linear potentiometer). The time delay between the piston speed and the corresponding flow speed at the rotor inlet, due to the presence of the chamber volume [51], has been taken into account to correctly evaluate the flow rate through the turbine. Expected uncertainties for the global measurements (torque, wall static pressures and piston position) are summarized in Table 2, together with the specifications of the used transducers.

Table 2
Specifications of instrumentation used (FSS stands for Full Scale Span).

Measured variable	Sensor	Range	Accuracy
Wall static pressure at rig ambient side	Sensor technics BSDX series	±1 kPa	±1% FSS
Wall static pressure at rig piston side	Sensor technics BSDX series	±1 PSI	±0.5% FSS
Output torque	ETH messtechnik DRFL-I	±2 Nm	±0.1% FSS
Piston position	MAFEurope - DWT series	±1.5 m	±0.5% FSS
Turbine rotational speed	ETH messtechnik DRFL-I	±10 000 rpm	±1/60 rpm

All the rotors have been characterized in terms of their global performance, introduced in Section 2, under regular wave conditions. A sinusoidal piston motion has been reproduced inside the OWC chamber, with a maximum amplitude of 900 mm. The rotational speed, maintained fixed during each test, has been set to a value that allowed all turbines to be tested under the same Reynolds' number, calculated based on the blade chord (Re_c) as in Eq. (7), for any given flow condition. This point is particularly important given the strong dependency of turbomachinery performance (and lifting surfaces in general) on the value of the Reynolds' number, especially in the transitional range.

$$Re_c = \frac{\rho W_1 c}{\mu} = \frac{\rho U c}{\mu \cos(\beta_1)} = Re_{c,U}\sqrt{1+\phi^2} \tag{7}$$

Fig. 6. Pictures of the three tested rotors.

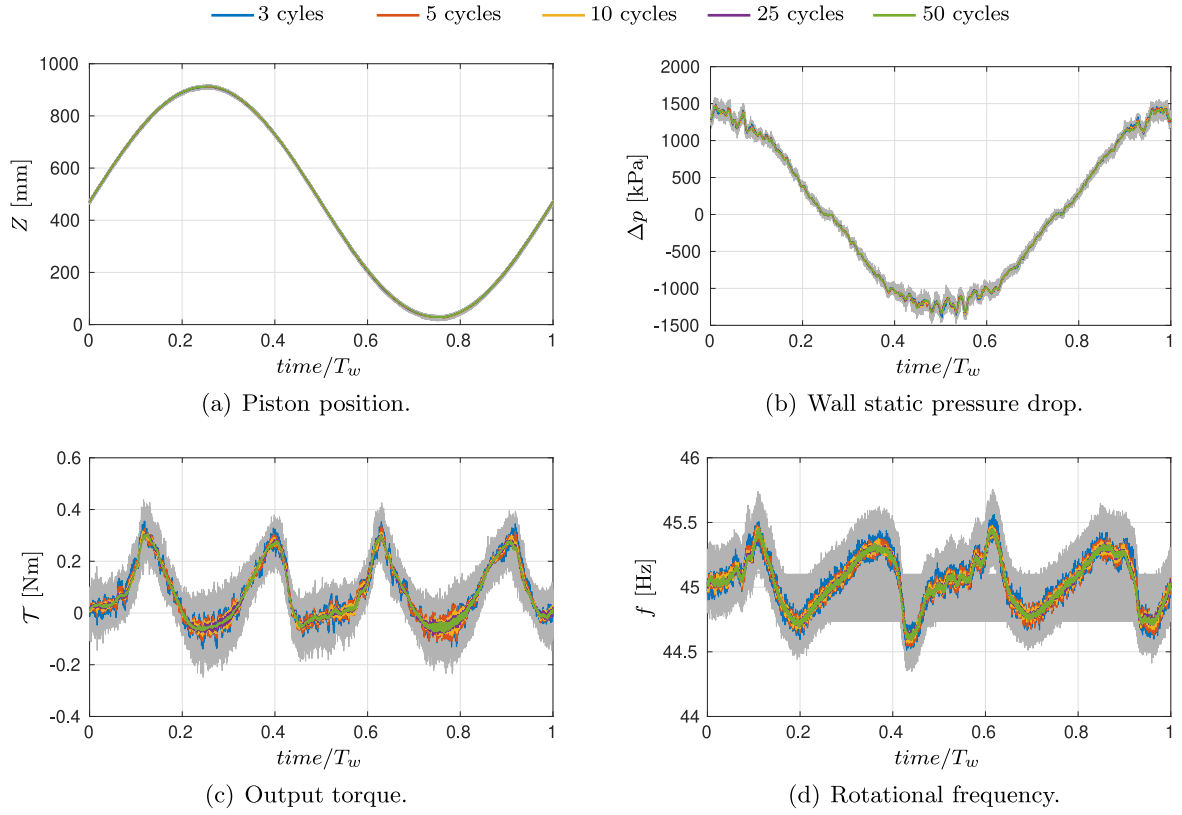

(a) Piston position. (b) Wall static pressure drop.

(c) Output torque. (d) Rotational frequency.

Fig. 7. Measured quantities in successive tests (gray lines) and data-reduction result considering a different number of piston periods.

In Eq. (7), $\beta_1 = \arctan(\phi)$ is the relative flow angle at the inlet of the rotor for a fully axial flow, as during the inflow phase (see Fig. 2). The experiments have been performed at a fixed value of $Re_{c,U}$ of 1.3×10^5 (the Reynolds' number calculated based on the chord and the peripheral velocity), with a maximum deviation of ±3%. In all experiments, the actual Reynolds' number Re_c varies depending on the flow coefficient, according to the right hand side of Eq. (7). The difficulty of performing experiments at a fixed Reynolds' number has been noted as one of the main limitations of the previous analyses [19]. The piston period has been adjusted in order to have, for every test, a range of flow coefficients that extended beyond the occurrence of stall. A detailed definition of the effective operating conditions each geometry has been tested at is reported in Table 3.

The overall sampling time for each test has been set to record signals for at least 5 piston periods with a sampling a rate of 1 kHz. An average distribution of the acquired signals was obtained with a phase locked averaging process based on piston position. This allowed to obtain signals at a reduced number of points (250 points per period) for the global measured quantities. A preliminary test has been conducted to evaluate the effect of the number of periods used in the phase averaging process, as shown in Fig. 7.

Table 3
Operating conditions set for each rotor geometry.

Test	Rotor	t_c [%]	$\overline{AR}$	Turbine rotational speed [rpm]	Sinusoidal piston period [s]
1		0.5		2100	11.4
2	1	1.5	0.42	2100	10.3
3		2.5		2400	8.3
4		0.5		3300	8.3
5	2	1.5	0.70	3000	8.3
6		2.5		3000	8.3
7		0.5		4800	7.3
8	3	1.5	0.99	4800	6.2
9		2.5		4800	5.7

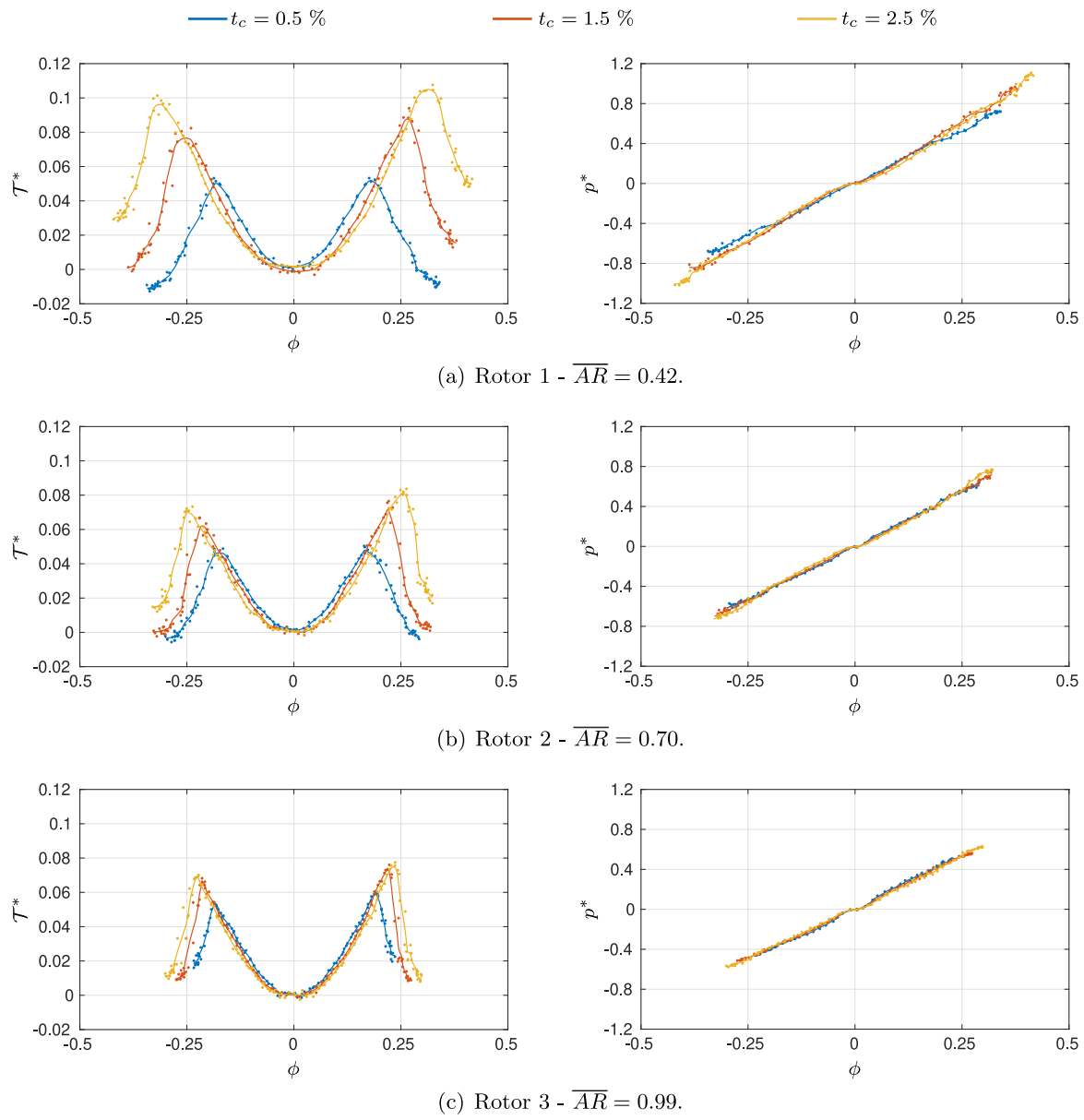

Fig. 8. Torque (left) and pressure (right) coefficients as a function of the flow coefficient for all the tested geometries (dots corresponds to the measurement points).

It should be noted that 5 periods can be considered sufficient for a good result of the phase averaging process of the acquired signals, also for the torque signal and the rotational frequency that presents larger fluctuations than other signals. This behavior was expected due to the nature of these signals and the high sensitivity of the torquemeter to vibrations and electrical noise. The torque signal bandwidth becomes wider around zero values which are associated to piston inversions and turbine stall, the most critical conditions for torque measurements. However, the same conditions have a very limited impact on the problems studied in this work, i.e. the mean efficiency and stall point. It should be also noted that the reduction to 250 points (it has been done for any number of cycle considered in Fig. 7) does not sensibly modify the signals evolution in a piston period.

Starting from the phase averaged signals of Fig. 7, the performance parameters of Eqs. ((1), (2)) were evaluated and their maximum uncertainties estimated applying the uncertainty propagation method (UPM) to the overall measurements just before the stall point. As a result, the torque coefficient T^* shows a maximum uncertainty of ±9.8%, a value of ±1.0% has been evaluated for p^* and a value of ±1.6% for ϕ, while a slightly larger value of ±9.95% has been calculated for the efficiency η, that was evaluated as a function of the other non-dimensional parameters (2).

4. Results

For each rotor configuration, the characteristic curves have been evaluated based on the non-dimensional parameters defined in Eq. (1), and they are reported in Fig. 8.

By observing the $\phi - p^*$ curves on the right of Fig. 8, it can be deduced how the tip clearance size has a limited effect on the slope of the pressure coefficient curve, hence the rotor damping is only marginally influenced by this parameter. Also the variation in blade aspect ratio has a very small effect on the turbine damping, which is substantially the same for the three tested geometries. This result confirms what already observed in [18,40,52], showing how the turbine damping, which represents the slope of the characteristic curve, is mostly governed by the rotor solidity and only marginally by others geometric parameters. In order to better observe how the damping coefficient varies for the tested geometries, Fig. 9 shows the ratio of

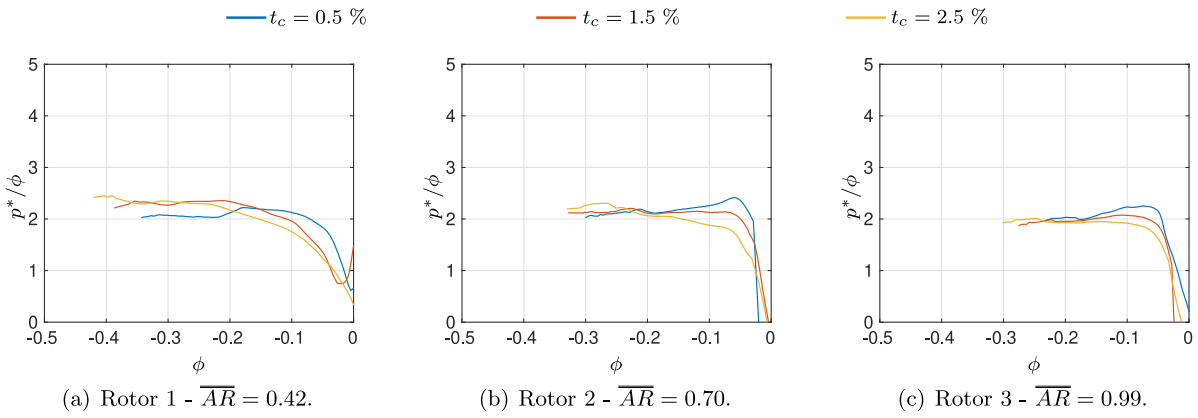

(a) Rotor 1 - $\overline{AR} = 0.42$. (b) Rotor 2 - $\overline{AR} = 0.70$. (c) Rotor 3 - $\overline{AR} = 0.99$.

Fig. 9. Damping coefficient as a function of the flow coefficient for all the tested geometries.

p^*/ϕ as a function of the flow coefficient, considering only the inflow phase (negative values of ϕ), in order to avoid the effect of the inlet swirling flow during the outflow phase.

It is evident how the damping is almost constant for the different geometries, with the exception of the operating conditions corresponding to very low flow coefficient (below 0.1). This more detailed analysis on this truly important parameter, fundamental to correctly couple a Wells turbine with an OWC chamber, confirms its limited variability with both t_c and AR. Nevertheless, for low values of the aspect ratio, Fig. 9(a), small variations of the damping coefficient can be appreciated with t_c, and this can be reasonably associated to a higher obstruction offered by the rotor. For larger values of AR, Fig. 9(b–c), a unique trend cannot be discerned for the tip gap-to-chord ratio, that does not appear to play a significant role in modifying the rotor obstruction on the flow, at least in the range of t_c values tested.

On the contrary, the stall onset is strongly controlled by the value of t_c. The tip vortex energizes the boundary layer on the suction side of the blades and larger values of the tip clearance increase the stable operating range of the turbine, delaying stall, as previously observed in [9,10,14]. This is clear from the torque coefficient curves on the left of Fig. 8. A similar effect is associated to the variation of the blade aspect ratio AR, although this value has a less marked influence on the stall onset. The asymmetry of performance curves between inflow (negative values of ϕ) and outflow (positive values of ϕ) phases can be observed for all the tested geometries, and it is linked to the presence of a swirled flow inside the chamber upstream of the turbine during the outflow phases, as shown in [43,44,51].

To evaluate the combined effects of t_c and AR the value of the flow coefficient at stall, ϕ_s, and the mean aerodynamic efficiency during a wave period are, typically, taken into account. In the present work, these two parameters have been evaluated only considering the inflow phase. The value of ϕ_s was evaluated from the data reported in Fig. 8, and it was assumed equal to the value of the flow coefficient at the maximum non-dimensional torque, after which $\mathcal{T}^*$ suddenly drops. The mean aerodynamic efficiency was calculated using Eq. (8), in the range $-\phi_s \leq \phi \leq 0$, i.e. the inflow stable operating range.

$$\overline{\eta} = \frac{\int_{T_{w,stable}} \mathcal{T}\,\Omega\,\mathrm{d}t}{\int_{T_{w,stable}} \Delta p Q\,\mathrm{d}t} \tag{8}$$

Fig. 10 shows both ϕ_s and $\overline{\eta}$ variations as a function of the aspect ratio, for the three values of t_c tested. For very low t_c values, the aspect ratio has a limited effect on the performance metrics. This is evident for the stall point, ϕ_s, which attains reasonably constant values when t_c is the lowest (line with circles). A similarly flat trend can be observed for the mean efficiency, which shows only limited variations, less than 5%, for the smallest value of t_c. Then, as t_c grows, the stall point moves to larger values of ϕ, while the mean efficiency reduces. For the larger values of t_c, the blade aspect ratio variation plays a

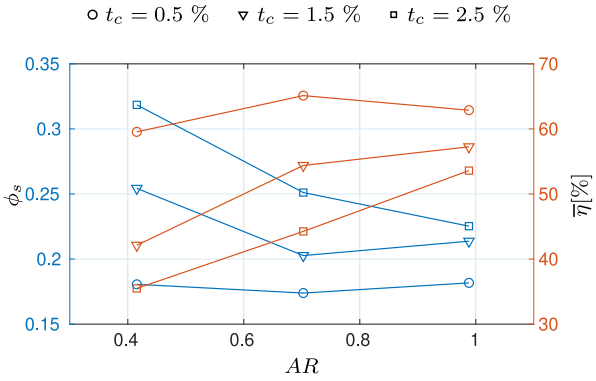

Fig. 10. Stall point and mean efficiency for the tested geometries, as a function of the blade aspect ratio.

role that is opposite to the one of t_c: while the mean efficiency grows with AR, the stall point is anticipated to lower flow rates. A possible explanation of these overall results can be given considering that for a fixed value of t_c, lower values of AR are associated to a larger tip gap size, that determines a larger flow through the tip gap that is able to energize the boundary layer on the suction side of the blade, producing a stall delay at the price of a penalty in efficiency. For the smallest values of t_c, the flow through the tip gap is probably not sufficient to provide this relief to the boundary layer. This aspect will be clarified later, with Fig. 12. In any case, the effects due to the tip gap-to-chord ratio on both the stall occurrence and the mean aerodynamic efficiency clearly dominate the effects due to the blade aspect ratio.

Although quantitative analyses on the mutual interaction between any PTO and OWC-based system require specific models for each component to be constructed [30,53], some considerations on the expected interaction can be reasonably drawn from the results of Figs. 9 and 10. Starting from the damping coefficient, which represents a key factor for the determination of the OWC chamber efficiency [54], results suggest a negligible dependence from the geometric parameters investigated in this work. In several works [29,31,55], its value is effectively varied by regulating the rotational speed to correctly match the desired behavior of an OWC chamber for a selected operating range. With this in mind, the definition of tip gap size and blade aspect-ratio values can be conducted finding a compromise between operating range limits, i.e. the flow coefficient at stall, and the turbine efficiency. The latter, often referred as “secondary stage” efficiency, has been observed to play a relevant role on the overall efficiency of the OWC system [30,56]. Finally, as the generator efficiency, also named “tertiary stage” efficiency, depends on the equilibrium of torque contributions at turbine–generator interface [57], an almost constant value

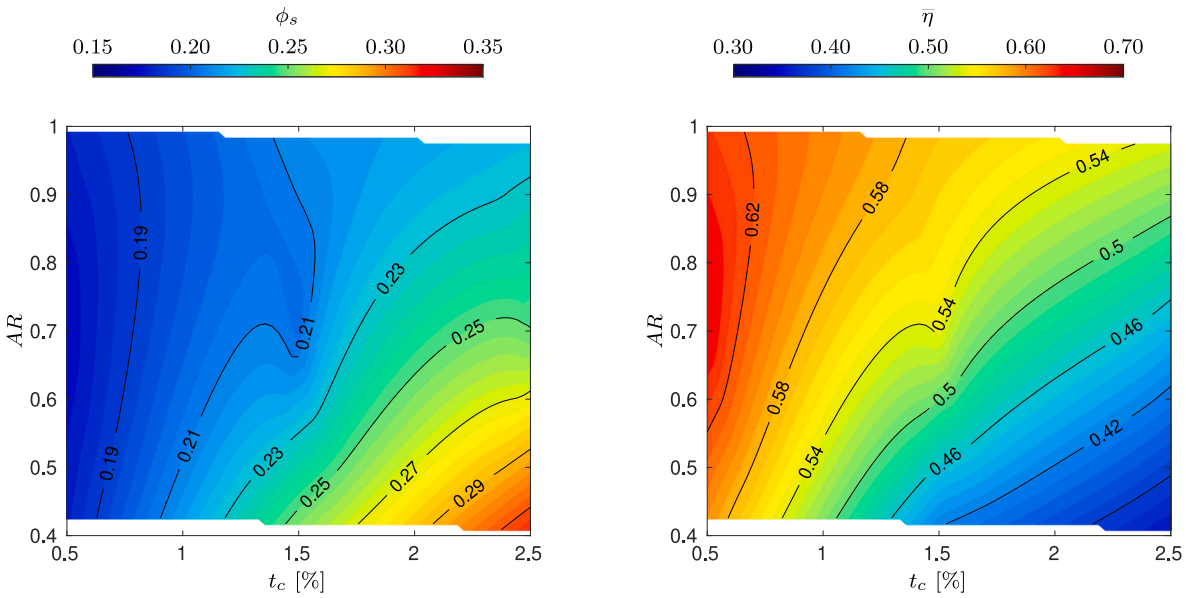

(a) Flow coefficient at the stall point. (b) Mean efficiency.

Fig. 11. Flow coefficient at stall and mean efficiency contour plots as a function of t_c and AR.

can be expected among all the tested geometries, given the substantially constant rotor inertia mostly governed by the hub geometry (the same for all tested geometries).

The trends of Fig. 10 are in agreement with the results presented by Raghunathan [19,49], in particular the curves for $t_c = 0.5\%$ (lines with circles), although the older data could be affected by the varying Reynolds' number, as stated by the authors. Also the consideration on the growing effect of the aspect ratio with larger tip gap-to-chord ratios, presented in [19], is clearly verified by these experimental data.

The contour plots in Fig. 11 provide a more readable representation of the combined influence of t_c and AR on efficiency and stall point. For small values of t_c, the examined performance metrics are independent from AR. For larger values of t_c, the relative influence of AR grows progressively. The effect of t_c is small for larger aspect ratio (relatively tall) blades, while it becomes progressively larger for small aspect ratio (relatively short) blades.

In order to verify whether the stall delay provided by aspect ratio blades is due solely to the larger tip gap size or also to other causes, flow coefficient at stall and mean efficiency have been also plotted as a function of tip gap-to-blade height ratio (t_h) and AR. This has been done in an attempt to find the most appropriate non-dimensionalization of the tip gap (gap-to-chord t_c or gap-to-height t_h) for analyzing the machine's performance. The results are presented in Fig. 12 in terms of contour plots.

These figures show that for a fixed value of t_h both stall point and mean efficiency do not sensibly vary with the AR, while increasing the t_h value provides a re-energization of the boundary layer on the suction side of the blade, thus delaying stall at the price of a lower efficiency. With this representation, the effects associated to the tip clearance size are separated from the ones due to the blade aspect ratio, showing an interesting insight, useful to design the Wells rotor. In fact, while the tip gap to blade height represents a compromise between the stall margin, the mean efficiency maximization and the practical construction of the rotor, the choice of the aspect ratio appears not to influence the performance of the machine significantly. While the tests presented in this study have been conducted at a fixed Reynolds' number, in order to isolate the effects of tip gap and aspect ratio, it is important to note how in a real installation the required turbine damping is likely to drive the rotor selection, hence turbines with lower AR would likely operate at larger Reynolds' numbers. The effect of this important parameter was therefore been investigated on a few selected geometries and it will be discussed in the next section.

4.1. Reynolds' number effects

The experiments presented in this work have been conducted at a fixed Reynolds' number, in order to allow the effects of tip gap and AR to be isolated and quantified. The value chosen for the Reynolds' number is 1.3×10^5, and it was dictated by the experimental setup limitations.

To understand the effects of this important flow parameter on Wells turbine performance, experiments were conducted for a single rotor (Rotor 3 in Table 1), by varying the Reynolds' number $Re_{c,U}$ in a range between 6×10^4 and 1.3×10^5. The results are reported in Fig. 13 for 3 values of the t_c.

The results in Fig. 13(a) show an approximately linear increase of the stall angle with the Reynolds' number that is compatible with a stall mechanisms dictated by a transitional boundary layer separation [58]. As the Reynolds' number grows, the boundary layer is capable to withstand larger angles of attack [58,59]. This stall mechanism is also in agreement with the numerical simulations in [60], conducted on a Wells turbine operating in the same range of Reynolds' number as the ones used in the present work.

On the other hand, the results in Fig. 13(b) suggest that Reynolds' number effects on $\overline{\eta}$ are not significant in the explored range of $Re_{c,U}$, showing an almost constant value of $\overline{\eta}$, with maximum variations smaller than 2%. To clarify this effect, Fig. 14 presents the variation in efficiency with flow coefficient for rotor 3 during the inflow phase and up to the occurrence of stall.

These representations show an almost flat trend of the aerodynamic efficiency with the flow coefficient, except near the inversion ($\phi = 0$). As the Reynolds' number grows, stall is delayed, but the efficiency value remains almost constant. Only small discrepancies from this behavior can be observed for test cases conducted at $Re_c = 0.63 \times 10^5$, probably affected by the larger uncertainty for measurements collected in the presence of low signal values. This behavior leads to an approximately constant value of the mean efficiency $\overline{\eta}$ for turbines operating at different Reynolds' numbers. This can be reasonably considered valid also for plant-scale turbines that typically operate at larger values of $Re = 0.5 - 2 \times 10^6$ [61].

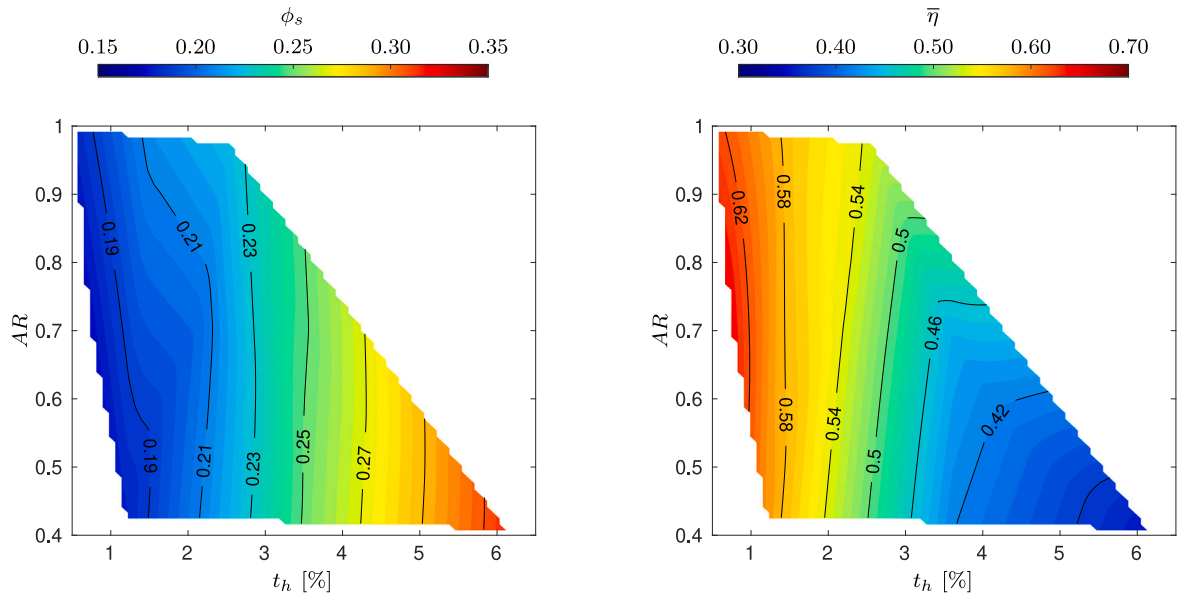

(a) Flow coefficient at the stall point. (b) Mean efficiency.

Fig. 12. Flow coefficient at stall and mean efficiency contour plots as a function of t_h and AR.

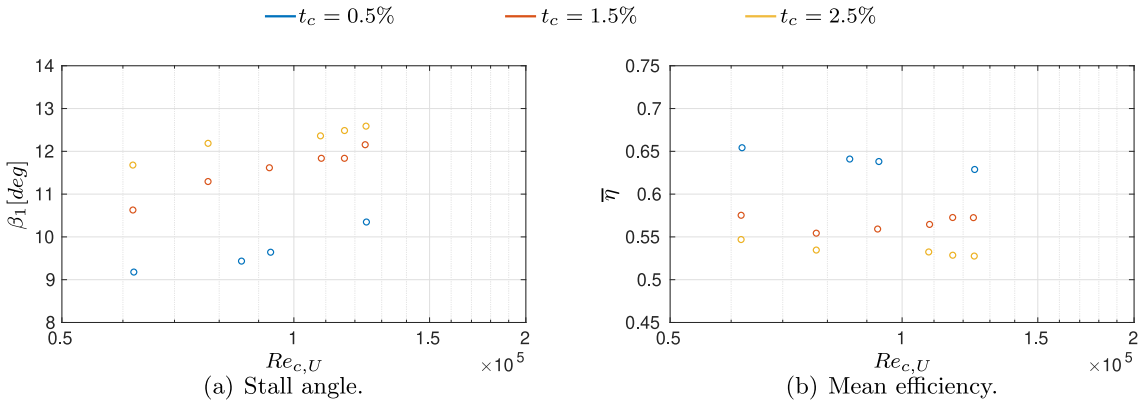

(a) Stall angle. (b) Mean efficiency.

Fig. 13. Reynolds' number effect for the Rotor 3.

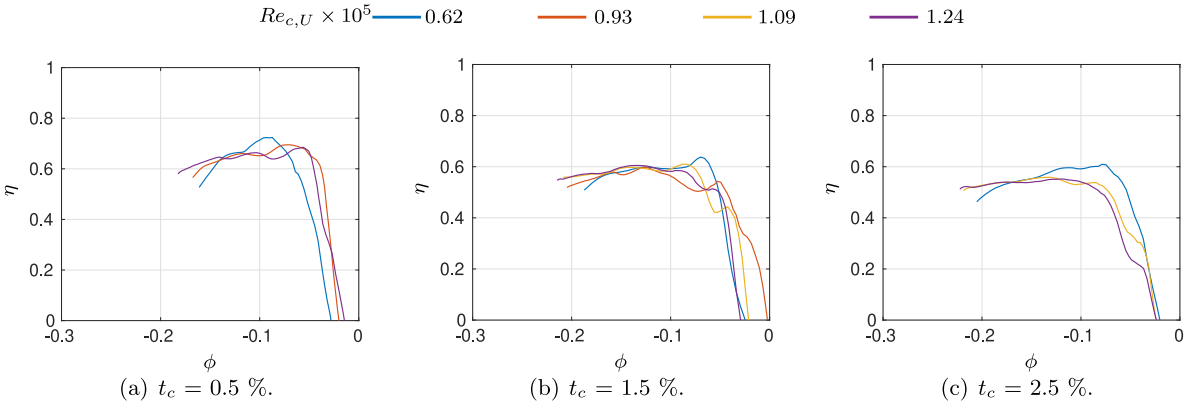

(a) $t_c = 0.5$ %. (b) $t_c = 1.5$ %. (c) $t_c = 2.5$ %.

Fig. 14. Aerodynamic efficiency as the function of the flow coefficient for Rotor 3.

4.2. Losses decomposition

As already discussed in Section 2, the total-to-static formulation of the efficiency, presented in Eq. (3), can be considered a more appropriate measure of the fraction of available energy converted into mechanical energy by the turbine. This evaluation has been done using the losses decomposition method, i.e. evaluating rotor and exit kinetic energy losses as described in [41,44]. Maps of Fig. 15 show the contour plots of loss coefficients averaged on a wave period (as done for the mean efficiency $\overline{\eta}$), as a function of t_h and AR.

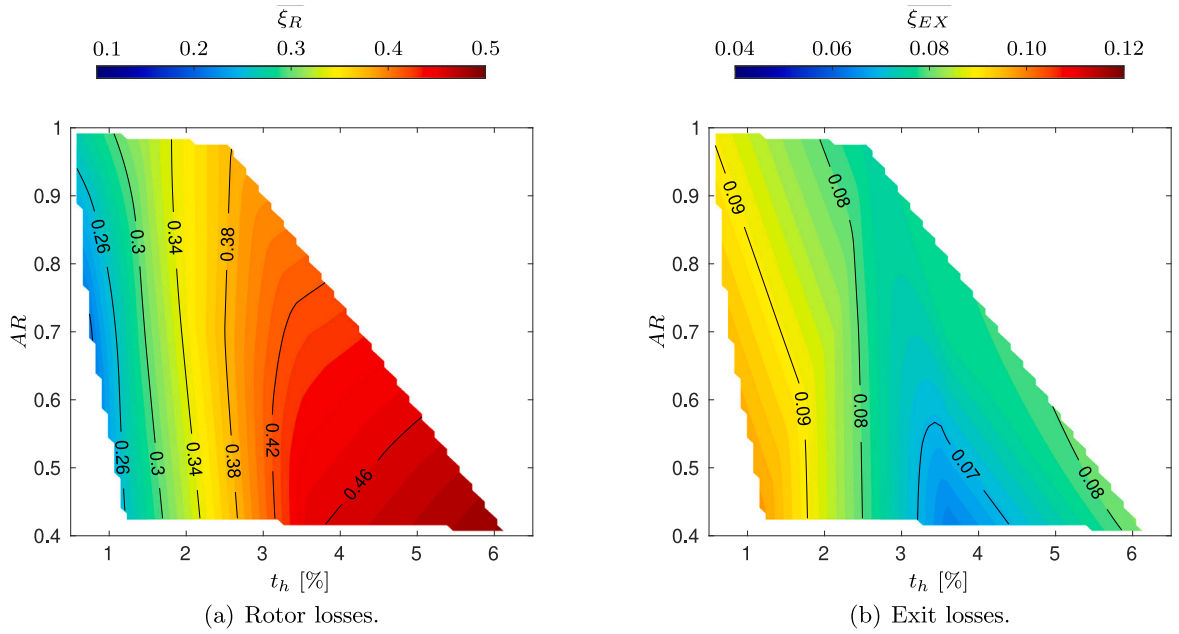

(a) Rotor losses. (b) Exit losses.

Fig. 15. Contours of the mean contributions of losses.

The losses decomposition clearly shows that the contribution due to the exit kinetic energy is small when compared to the rotor losses and almost constant in the ranges of variation considered for t_h and AR. Lower values are found for $t_h = 3$–4% and $AR = 0.4$–0.6, although the largest values are only marginally higher than these.

The substantially constant value of $\overline{\xi_{EX}}$ in Fig. 15(b) suggests that exit kinetic energy losses are only marginally influenced by the tip clearance and the blade aspect ratio. This is in agreement with potential flow analysis on blade profiles with negligible thickness [19,62], based on which the absolute exit flow angle α_2 depends only on the rotor solidity, and so does the exit kinetic energy for a fixed operating condition. On the other hand, relevant variations can be observed for the rotor losses, ξ_R, which are representative of the weighted aerodynamic losses through the rotor, as demonstrated in [41]. In particular, ξ_R variations are strongly dominated by the tip gap-to-height value, while AR starts to influence the rotor losses only for values of t_h larger than 3%–4%. Similar trends were also reported in [19].

Finally, combining rotor and exit kinetic energy losses as in Eq. (3), the mean total-to-static efficiency can be calculated. A map of $\overline{\eta_{ts}}$ is shown in Fig. 16, as a function of t_h and AR values. As expected, the total-to-static efficiency map appears not too dissimilar from the map of the rotor losses given in Fig. 15(a), showing almost the same trend of contour lines. As it was the case for the aerodynamic efficiency (Fig. 12(b)), also the total-to-static efficiency depends on the value of t_h, while the effect of AR is limited. Maximum values are observed for the lowest t_h values, where the rotor losses are the lowest although exit kinetic energy losses are the highest. This is a confirmation of the relative weight of rotor losses contribution that was observed for a fixed rotor in [41,63] and now generalized in the investigated range of variation of AR and t_h.

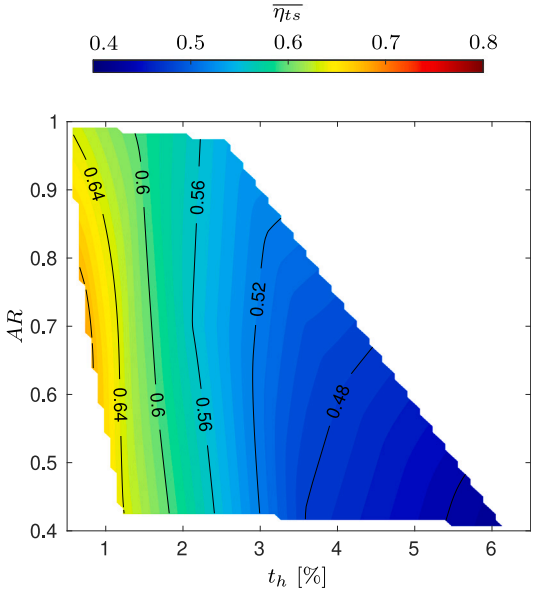

Fig. 16. Contours of the mean total-to-static efficiency.

5. Conclusions

This work provides an experimental investigation on the effects of tip clearance and blade aspect ratio on Wells rotor performance. The investigation has been conducted on a Wells turbine prototype coupled to an OWC simulator that reproduces regular wave conditions, allowing to evaluate the global performance in a wide operating range extending after stall. The geometric parameters investigated, i.e. the tip clearance size and the blade aspect ratio, have been varied by testing a total number of 9 rotors, with particular attention to preserve the remaining geometric and flow parameters as constant as possible, in order to correctly separate and evaluate their influence. Given the importance of the Reynolds' number on both stall occurrence and rotor performance, its value has been kept fixed for all the 9 geometries, while for some selected rotors its effect has been investigated with additional tests. The main findings of this experimental investigation are:

- The tip clearance size plays a dominant role on both the stall point and the rotor performance, in particular the efficiency. The aspect ratio plays a less relevant role, which becomes noticeable only for large values of the tip clearance size. The aspect ratio has also a small effect on the turbine damping while the tip clearance size does not affect the slope of the $p^* - \phi$ rotor characteristic, at least in the investigated range of variation for t_c.

- A clear separation of the effects due to the tip gap and the aspect ratio is observed when the former parameter is non-dimensionalized with respect to the blade height (t_h) rather than to the chord (t_c), as typically found in literature. Using this formulation, it has been observed that the stall occurrence does not depend on the value of the aspect ratio, but only on the relative tip gap size which modifies the stable range of the turbine and its efficiency.
- The non-dimensional damping coefficient shows almost negligible variations with both the tip gap size and the aspect ratio value. This represents a useful information for the evaluation of OWC-Wells turbine coupling and mutual interaction by means of lower-order models such as wave-to-wire ones.
- For a given geometry, the Reynolds' number has been observed to play a significant role on the stall point, extending the stable operating range as it becomes larger. This effect has been verified only for moderate values of the Reynolds' number, due to the limitations of the experimental setup. The investigated values are however not too dissimilar from the ones found in the literature for experimental tests. The reduced variation of the aerodynamic efficiency with the Reynolds' number suggests that these can be extended to real scale rotors, without expecting any relevant variations.
- Rotor losses are mainly driven by the tip gap to height parameter, while the exit losses are approximately constant in the investigated range of parameters. The former are predominant with respect to the latter for each rotor configuration and their trends drive the total-to-static efficiency, which results from the combination of these two loss contributions. Exit kinetic energy losses are only marginally affected by both the investigated parameters, suggesting that they might be driven by other geometric parameters, such as the rotor solidity.

The set of experimental data presented within this work can be, in the authors' opinion, an useful benchmark to extend parametric analyses on the geometry of the Wells turbine, using also numerical approaches. Further investigations should be oriented to investigate other relevant geometric parameters, such as the solidity and the hub-to-tip ratio of the rotor, in order to give a complete description of the turbine geometry affects the Wells turbine performance and to provide correlations useful to drive the turbine design. Moreover, the experimental Wells turbine characteristics presented in this work can be directly used in existing models that reproduce the performance of an oscillating water column system, in order to evaluate its overall performance in the presence of different rotor geometries, in order to properly select the best combination of OWC and turbine for the required operating conditions or sea states.

CRediT authorship contribution statement

Fabio Licheri: Writing – review & editing, Writing – original draft, Visualization, Software, Methodology, Investigation, Formal analysis, Data curation, Conceptualization. **Tiziano Ghisu:** Writing – review & editing, Visualization, Supervision, Data curation, Conceptualization. **Francesco Cambuli:** Writing – review & editing, Supervision, Project administration, Funding acquisition, Conceptualization. **Pierpaolo Puddu:** Writing – review & editing, Visualization, Supervision, Methodology, Data curation, Conceptualization. **Mario Carta:** Writing – review & editing.

Funding

This study was carried out by Fabio Licheri within the "e.INS - Ecosystem of Innovation for Next Generation Sardinia" funded by the Italian Ministry of University and Research under the Next-Generation EU Programme (National Recovery and Resilience Plan - PNRR, M4C2, INVESTMENT 1.5 - DD 1056 of 23/06/2022, ECS00000038). This manuscript reflects only the authors' views and opinions, neither the European Union nor the European Commission can be considered responsible for them.

Francesco Cambuli acknowledges financial support under the National Recovery and Resilience Plan (NRRP), Mission 4, Component 2, Investment 1.1, Call for tender No 1409, published on 14.9.2022 financed by the Italian Ministry of University and Research, funded by the European Union - Next-GenerationEU - Project Title APEIRON - CUP F53D23009560001 - Grant Assignment Decree No. 0001385 adopted on 01-09-2023 by the Italian Ministry of University and Research, and by the National Recovery and Resilience Plan (NRRP), Mission 4, Component 2, Investment 1.3, Call for Tender No. 1561 dated October 11, 2022, PE_0000021, financed by the Italian Ministry of University and Research, funded by the European Union - Next-GenerationEU - Project Title "Network 4 Energy Sustainable Transition NEST"

Pierpaolo Puddu and Tiziano Ghisu acknowledge financial support under the National Recovery and Resilience Plan (NRRP), Mission 4, Component 2, Investment 1.1, Call for tender No. 1409 published on 14.9.2022 by the Italian Ministry of University and Research (MUR), funded by the European Union - NextGenerationEU - Project Title APEIRON - CUP F53D23009560001 - Grant Assignment Decree No. 0001385 adopted on 01-09-2023 by the Italian Ministry of University and Research (MUR).

Declaration of competing interest

The authors declare the following financial interests/personal relationships which may be considered as potential competing interests: Fabio Licheri reports financial support was provided by Italian Ministry of University and Research. Tiziano Ghisu reports financial support was provided by Italian Ministry of University and Research. Francesco Cambuli reports financial support was provided by Italian Ministry of University and Research. Pierpaolo Puddu reports financial support was provided by Italian Ministry of University and Research. If there are other authors, they declare that they have no known competing financial interests or personal relationships that could have appeared to influence the work reported in this paper.

References

[1] World Energy Transitions Outlook 2023: 1.5°C Pathway, vol. 1, International Renewable Energy Agency, Abu Dhabi, 2023, https://mc-cd8320d4-36a1-40ac-83cc-3389-cdn-endpoint.azureedge.net/-/media/Files/IRENA/Agency/Publication/2023/Jun/IRENA_World_energy_transitions_outlook_2023.pdf?rev=db3ca01ecb4a4ef8accb31d017934e97.

[2] Ocean Energy Stats & Trends 2023, Ocean Energy Europe, 2024, https://www.oceanenergy-europe.eu/category/publication-library/.

[3] G. Besio, L. Mentaschi, A. Mazzino, Wave energy resource assessment in the mediterranean sea on the basis of a 35-year hindcast, Energy 94 (2016) 50–63, http://dx.doi.org/10.1016/j.energy.2015.10.044.

[4] B. Guo, J.V. Ringwood, A review of wave energy technology from a research and commercial perspective, IET Renew. Power Gener. 15 (14) (2021) 3065–3090, http://dx.doi.org/10.1049/rpg2.12302.

[5] T.V. Heath, A review of oscillating water columns, Phil. Trans. R. Soc. A 370 (1959) (2012) 235–245, http://dx.doi.org/10.1098/rsta.2011.0164.

[6] A. Wells, Fluid driven rotary transducer - BR. Pat. 1595700, 1976.

[7] A. Shehata, Q. Xiao, K. Saqr, D. Alexander, Wells turbine for wave energy conversion: A review, Int. J. Energy Res. 41 (1) (2017) 6–38, http://dx.doi.org/10.1002/er.3583.

[8] J. Watterson, M. Gillan, S. Raghunathan, R. Mitchell, Applications of computational fluid dynamics to a wave energy conversion device, in: IECEC-97 Proceedings of the Thirty-Second Intersociety Energy Conversion Engineering Conference (Cat. No.97CH6203), vol.3, vol. 3, 1997, pp. 1976–1981, http://dx.doi.org/10.1109/IECEC.1997.656729.

[9] J. Watterson, S. Raghunathan, Computed effects of tip clearance on Wells turbine performance, in: 35th Aerospace Sciences Meeting and Exhibit, 1997, http://dx.doi.org/10.2514/6.1997-994.

[10] Z. Taha, Sugiyono, T. Sawada, A comparison of computational and experimental results of Wells turbine performance for wave energy conversion, Appl. Ocean Res. 32 (1) (2010) 83–90, http://dx.doi.org/10.1016/j.apor.2010.04.002.

[11] T.H. Kim, Y. Kinoue, T. Setoguchi, K. Kaneko, Effects of hub-to-tip ratio and tip clearance on hysteretic characteristics of Wells turbine for wave power conversion, J. Therm. Sci. 11 (2002) 207–213, http://dx.doi.org/10.1007/s11630-002-0056-7.

[12] M. Takao, T. Setoguchi, S. Nagata, K. Toyota, A Study on the Effects of Blade Profile and Non-Uniform Tip Clearance of the Wells Turbine, in: International Conference on Offshore Mechanics and Arctic Engineering, Volume 6: Nick Newman Symposium on Marine Hydrodynamics; Yoshida and Maeda Special Symposium on Ocean Space Utilization; Special Symposium on Offshore Renewable Energy, 2008, pp. 625–632, http://dx.doi.org/10.1115/OMAE2008-57235.

[13] Z. Taha, Sugiyono, T.M.Y.S. Tuan Ya, T. Sawada, Numerical investigation on the performance of Wells turbine with non-uniform tip clearance for wave energy conversion, Appl. Ocean Res. 33 (4) (2011) 321–331, http://dx.doi.org/10.1016/j.apor.2011.07.002.

[14] M. Torresi, S. Camporeale, P. Strippoli, G. Pascazio, Accurate numerical simulation of a high solidity Wells turbine, Renew. Energy 33 (4) (2008) 735–747, http://dx.doi.org/10.1016/j.renene.2007.04.006.

[15] K. Vafiadis, A. Tourlidakis, A. Krikas, Computational Analysis of a Wells Turbine for Wave Power Generation, in: Proceedings of Global Power and Propulsion Society, GPPS Chania 20, Sept. 7–9, 2020, http://dx.doi.org/10.33737/gpps20-tc-129.

[16] M. Suzuki, C. Arakawa, T. Tagori, Fundamental studies on Wells turbine for wave power generator (1st report, the effect of solidity, and self-starting), Bull. JSME 27 (231) (1984) 1925–1931, http://dx.doi.org/10.1299/jsme1958.27.1925.

[17] Y.M. Ahmed, O. Yaakob, A.H. Elbatran, U.J.A. Mazukee, Wells turbine for wave energy conversion for Malaysian ocean, J. Ocean. Mech. Aerosp. - Sci. Eng. 8 (2014) 12–16.

[18] J. Watterson, S. Raghunathan, Computed effects of solidity on Wells turbine performance, JSME Int. J. Ser. B: Fluids Therm. Eng. 41 (1) (1998) 177–183, http://dx.doi.org/10.1299/jsmeb.41.177.

[19] S. Raghunathan, The Wells air turbine for wave energy conversion, Prog. Aerosp. Sci. 31 (4) (1995) 335–386, http://dx.doi.org/10.1016/0376-0421(95)00001-F.

[20] M. Takao, T. Setoguchi, Y. Kinoue, K. Kaneko, Wells turbine with end plates for wave energy conversion, Ocean Eng. 34 (11) (2007) 1790–1795, http://dx.doi.org/10.1016/j.oceaneng.2006.10.009.

[21] K. Takasaki, T. Tsunematsu, M. Takao, M.M.A. Alam, T. Setoguchi, Wells turbine for wave energy conversion - effect of trailing edge shape, Int. J. Fluid Mach. Syst. 9 (4) (2016) 307–312, http://dx.doi.org/10.5293/IJFMS.2016.9.4.307.

[22] A. Shehata, Q. Xiao, M. Selim, A. Elbatran, D. Alexander, Enhancement of performance of wave turbine during stall using passive flow control: First and second law analysis, Renew. Energy 113 (2017) 369–392, http://dx.doi.org/10.1016/j.renene.2017.06.008.

[23] T. Gratton, T. Ghisu, G. Parks, F. Cambuli, P. Puddu, Optimization of blade profiles for the Wells turbine, Ocean Eng. 169 (2018) 202–214, http://dx.doi.org/10.1016/j.oceaneng.2018.08.066.

[24] M. Nazeryan, E. Lakzian, Detailed entropy generation analysis of a Wells turbine using the variation of the blade thickness, Energy 143 (2018) 385–405, http://dx.doi.org/10.1016/j.energy.2017.11.006.

[25] P.M. Kumar, P. Halder, A. Samad, Performance Analysis of Wells Turbine with Radiused Blade Tip, in: International Conference on Offshore Mechanics and Arctic Engineering, Volume 10: Ocean Renewable Energy, 2018, http://dx.doi.org/10.1115/omae2018-78668.

[26] P.M. Kumar, A. Samad, Introducing gurney flap to Wells turbine blade and performance analysis with OpenFOAM, Ocean Eng. 187 (2019) 106212, http://dx.doi.org/10.1016/j.oceaneng.2019.106212.

[27] T.K. Das, A. Samad, Influence of stall fences on the performance of Wells turbine, Energy 194 (2020) 116864, http://dx.doi.org/10.1016/j.energy.2019.116864.

[28] J. Henriques, J. Portillo, W. Sheng, L. Gato, A. Falcão, Dynamics and control of air turbines in oscillating-water-column wave energy converters: Analyses and case study, Renew. Sustain. Energy Rev. 112 (2019) 571–589, http://dx.doi.org/10.1016/j.rser.2019.05.010.

[29] L. Ciappi, L. Cheli, I. Simonetti, A. Bianchini, L. Talluri, L. Cappietti, G. Manfrida, Wave-to-wire models of Wells and impulse turbines for oscillating water column wave energy converters operating in the mediterranean sea, Energy 238 (2022) 121585, http://dx.doi.org/10.1016/j.energy.2021.121585.

[30] L. Ciappi, I. Simonetti, A. Bianchini, L. Cappietti, G. Manfrida, Application of integrated wave-to-wire modelling for the preliminary design of oscillating water column systems for installations in moderate wave climates, Renew. Energy 194 (2022) 232–248, http://dx.doi.org/10.1016/j.renene.2022.05.015.

[31] M. Rosati, J.V. Ringwood, Wave-to-wire efficiency maximisation for oscillating-water-column systems, IFAC- Pap. 56 (2) (2023) 10886–10891, http://dx.doi.org/10.1016/j.ifacol.2023.10.769, 22nd IFAC World Congress.

[32] W.K. Tease, J. Lees, A. Hall, Advances in oscillating water column air turbine development, in: Proceedings of the 7th European wave and tidal energy conference, Porto, Portugal, 2007.

[33] S.L. Dixon, C.A. Hall, Fluid Mechanics and Thermodynamics of Turbomachinery, Sixth ed., Elsevier, Inc., 2010.

[34] E. Dick, Fundamentals of Turbomachines, second ed., in: in Fluid Mechanics and Its Applications, Springer Cham, 2022, p. 600, http://dx.doi.org/10.1007/978-3-030-93578-8.

[35] L. Gato, A. de O. Falcão, Aerodynamics of the Wells turbine, Int. J. Mech. Sci. 30 (6) (1988) 383–395, http://dx.doi.org/10.1016/0020-7403(88)90012-4.

[36] M. Stefanizzi, S.M. Camporeale, M. Torresi, Experimental investigation of a Wells turbine under dynamic stall conditions for wave energy conversion, Renew. Energy 214 (2023) 369–382, http://dx.doi.org/10.1016/j.renene.2023.05.120.

[37] S. Raghunathan, C. Tan, N. Wells, Theory and performance of a Wells turbine, J. Energy 6 (2) (1982) 157–160, http://dx.doi.org/10.2514/3.48047.

[38] M. Folley, R. Curran, T. Whittaker, Comparison of LIMPET contra-rotating Wells turbine with theoretical and model test predictions, Ocean Eng. 33 (8) (2006) 1056–1069, http://dx.doi.org/10.1016/j.oceaneng.2005.08.001.

[39] T. Ghisu, F. Cambuli, P. Puddu, I. Virdis, M. Carta, F. Licheri, A lumped parameter model to explain the cause of the hysteresis in OWC-Wells turbine systems for wave energy conversion, Appl. Ocean Res. 94 (2020) http://dx.doi.org/10.1016/j.apor.2019.101994.

[40] F. Licheri, F. Cambuli, P. Puddu, T. Ghisu, A comparison of different approaches to estimate the efficiency of Wells turbines, J. Fluids Eng. 143 (5) (2021) http://dx.doi.org/10.1115/1.4049686.

[41] F. Licheri, T. Ghisu, F. Cambuli, P. Puddu, Detailed investigation of the local flow-field in a Wells turbine coupled to an OWC simulator, Renew. Energy 197 (2022) 583–593, http://dx.doi.org/10.1016/j.renene.2022.07.116.

[42] J. Horlock, Losses and efficiencies in axial-flow turbines, Int. J. Mech. Sci. 2 (1) (1960) 48–75, http://dx.doi.org/10.1016/0020-7403(60)90013-8.

[43] P. Puddu, M. Paderi, C. Manca, Aerodynamic Characterization of a Wells Turbine Under Bi-Directional Airflow, in: Energy Procedia, 68th Conference of the Italian Thermal Machines Engineering association, ATI2013, vol. 45, 2014, pp. 278–287, http://dx.doi.org/10.1016/j.egypro.2014.01.030.

[44] F. Licheri, T. Ghisu, F. Cambuli, P. Puddu, Experimental reconstruction of the local flow field in a Wells turbine using a three-dimensional pressure probe, Energy 296 (2024) 131062, http://dx.doi.org/10.1016/j.energy.2024.131062.

[45] R. Curran, L.M.C. Gato, The energy conversion performance of several types of Wells turbine designs, Proc. Inst. Mech. Eng. A 211 (2) (1997) 133–145, http://dx.doi.org/10.1243/0957650971537051.

[46] M. Govardhan, T. Dhanasekaran, Effect of guide vanes on the performance of a self-rectifying air turbine with constant and variable chord rotors, Renew. Energy 26 (2) (2002) 201–219, http://dx.doi.org/10.1016/S0960-1481(01)00124-0.

[47] A. Thakker, R. Abdulhadi, The performance of Wells turbine under bi-directional airflow, Renew. Energy 33 (11) (2008) 2467–2474, http://dx.doi.org/10.1016/j.renene.2008.02.013.

[48] S. Camporeale, P. Filianoti, Behaviour of a small Wells turbine under randomly varying oscillating flow, in: Proceedings of the 8th European Wave and Tidal Energy Conference, EWTEC, Uppsala, Sweden, 2009.

[49] S. Raghunathan, A methodology for Wells turbine design for wave energy conversion, Proc. Inst. Mech. Eng. A 209 (3) (1995) 221–232, http://dx.doi.org/10.1243/PIME_PROC_1995_209_040_02.

[50] F. Licheri, T. Ghisu, F. Cambuli, P. Puddu, Experimental analysis of the three-dimensional flow in a wells turbine rotor, Int. J. Turbomach. Propuls. Power 8 (3) (2023) http://dx.doi.org/10.3390/ijtpp8030021.

[51] M. Paderi, P. Puddu, Experimental investigation in a Wells turbine under bi-directional flow, Renew. Energy 57 (2013) 570–576, http://dx.doi.org/10.1016/j.renene.2013.02.016.

[52] F. Licheri, P. Puddu, F. Cambuli, T. Ghisu, Experimental Investigation on a Speed Controlled Wells Turbine for Wave Energy Conversion, in: International Conference on Offshore Mechanics and Arctic Engineering, Volume 8: Ocean Renewable Energy, 2022, V008T09A077, http://dx.doi.org/10.1115/OMAE2022-80986.

[53] L. Ciappi, M. Stebel, J. Smolka, L. Cappietti, G. Manfrida, Analytical and computational fluid dynamics models of Wells turbines for oscillating water column systems, J. Energy Resour. Technol. 144 (5) (2021) 050903, http://dx.doi.org/10.1115/1.4052216.

[54] H. Bouhrim, A. El Marjani, Effects of turbine damping and wave conditions on OWC performances for optimal wave energy conversion, J. Ocean Eng. Mar. Energy 9 (5) (2023) 697–713, http://dx.doi.org/10.1007/s40722-023-00293-y.

[55] B. Fenu, J.C. Henriques, M. Glorioso, L.M. Gato, M. Bonfanti, Real-time Wells turbine simulation on an oscillating-water-column wave energy converter physical model, Appl. Energy 376 (2024) 124121, http://dx.doi.org/10.1016/j.apenergy.2024.124121.

[56] T. Murakami, Y. Imai, S. Nagata, M. Takao, T. Setoguchi, Experimental research on primary and secondary conversion efficiencies in an oscillating water column-type wave energy converter, Sustainability 8 (8) (2016) http://dx.doi.org/10.3390/su8080756.

[57] L. Ciappi, L. Cheli, I. Simonetti, A. Bianchini, G. Manfrida, L. Cappietti, Wave-to-wire model of an oscillating-water-column wave energy converter and its application to mediterranean energy hot-spots, Energies 13 (21) (2020) http://dx.doi.org/10.3390/en13215582.

[58] S. Wang, Y. Zhou, M.M. Alam, H. Yang, Turbulent intensity and Reynolds number effects on an airfoil at low Reynolds numbers, Phys. Fluids 26 (11) (2014) 115107, http://dx.doi.org/10.1063/1.4901969.

[59] E.N. Jacobs, A. Sherman, Airfoil Section Characteristics as Affected by Variations of the Reynolds Number, Tech. Rep. 586, NACA, 1939.

[60] M. Torresi, S. Camporeale, G. Pascazio, Detailed CFD analysis of the steady flow in a Wells turbine under incipient and deep stall conditions, J. Fluids Eng. Trans. ASME 131 (7) (2009) 0711031–07110317, http://dx.doi.org/10.1115/1.3155921.

[61] L. Gato, J. Henriques, A. Carrelhas, Sea trial results of the biradial and Wells turbines at mutriku wave power plant, Energy Convers. Manage. 268 (2022) 115936, http://dx.doi.org/10.1016/j.enconman.2022.115936.

[62] A.F.O. Falcão, L.M.C. Gato, 8.05 - Air Turbines, in: Comprehensive Renewable Energy, Elsevier, Oxford, 2012, pp. 111–149, http://dx.doi.org/10.1016/B978-0-08-087872-0.00805-2.

[63] F. Licheri, P. Puddu, T. Ghisu, F. Cambuli, Experimental analysis of the unsteady flow inside a Wells turbine, in: Proceedings of the 76th Italian National Congress ATI, Rome, Italy, vol. 312, 2021, p. 11009, http://dx.doi.org/10.1051/e3sconf/202131211009.